Pavement Roughness Estimation Using Path Tortuosity and 2-D Lacunarity Measure.

Arnaud LINA, Paul COHEN, Jean-Yves HERVÉ.
Perception and Robotics Laboratory, Department of Electrical and Computer Engineering
Ecole Polytechnique, Montreal H3C 3A7, Canada. *

March 13, 2000

Abstract

This paper presents two approaches to the estimation of pavement surface roughness from range data using profile tortuosity and fractal lacunarity. Estimations are performed on high frequency data components issued from pavements details. Based on the scale ratio of the distinct physical structures which composed the road surface, high frequency components are first recovered using a multiresolution decomposition. A Fisher-measure classification scheme is then employed to segment the pavement surface into regions of distinct roughness. The result is finally a segmented map of the road into sections of distinct qualitative roughness.

1 Introduction

Automated pavement surveying is becoming an important preoccupation of highway administration. To maintain current information about the spatial distribution of pavement quality of road networks, high-tech companies are now offering equipment for automated pavement data collection and processing. Some researchers [1, 2] have developed asphalt classification methods based upon optical images of the pavement. These methods do not, however, allow estimation of a high-resolution roughness characteristics. In this paper, we use telemetric data collected with a vehicle-mounted laser range-finder to measure pavement roughness. The vehicle developed by the firm GIE Technologies Inc. [4], uses bi-iris laser range-finders originally developed by the National Research Council of Canada [3]. At a vehicle speed of 60 km/h, each range-finder acquires road surface profiles separated by a 10 cm distance and consisting of 256 range values across a 90 cm road transversal distance. The profiles are referenced along the vehicle's path using GPS, odometric, and inertia data. Figures 1(a) and 1(b) illustrate the data collection process. The collected data consists of estimated distances between a sensor and the pavement surface. Since the geometry of the road surface and the spatial attitude of the vehicle are unknown, these elements cannot be completely separated. However, a multiresolution decomposition [6, 5] of the collected data is able to separate the low-frequency surface component resulting from the combination of the vehicle's attitude and of the road surface global geometry, from the high-frequency details associated with the pavement's texture. An example of this separation is shown in Figure 2. The surface data resulting from this separation process is characterized by a 3 mm transversal resolution and a 10 cm longitudinal resolution.

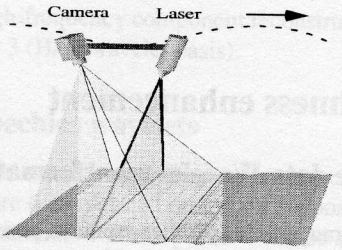

(a) ata acquisition principle.

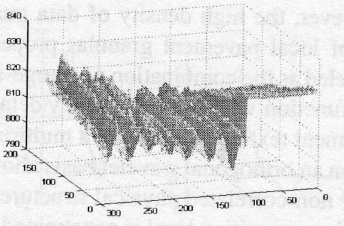

(b) xample of collected range data.

Figure 1: Surface data collection.

*This work has been supported by the ational Science and ngineering Research ouncil of anada under rant R 193570, and by ... Technologies nc., ontreal, anada.

To estimate the global and the local surface roughness, we introduce two types of measures, namely tortuosity and lacunarity. Measurements are, then, segmented to yield sections of pavement of distinct surface roughness indexed with odometric information.

This paper is organized as follows. Section 2 describes the Wavelet-based decomposition in order to extract the high-frequency component of the range data. Tortuosity and the lacunarity measures to charaterize the pavement roughness are described in Section 3. Section 4 presents a segmentation method based upon the Fisher classification method [7] to cluster the measures. Concluding remarks appear in Section 5.

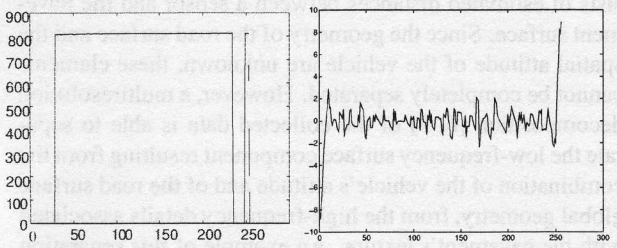

(a) Raw data. (b) igh-frequency component.

Figure 2: Example of range profile.

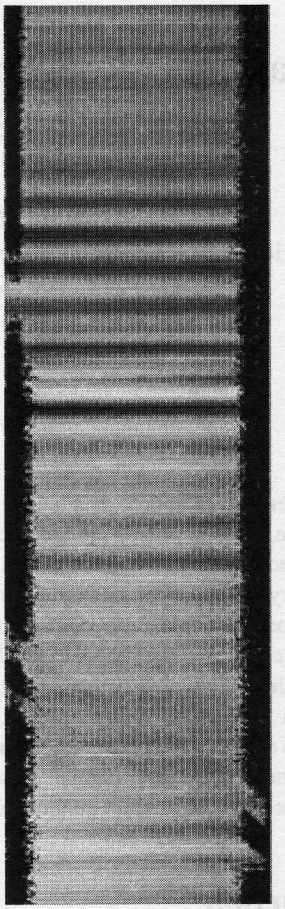

Figure 3: Example of raw data.

2 Roughness enhancement

2.1 Range data Wavelet transformation

The collected range-value profiles are, first, concatenated as shown in Figure 3. Low-frequency range variations result from the combined effects of sensor motion (including vibrations) and road geometry. This signal should therefore not be misunderstood as a reconstruction of the pavement's surface. However, the high density of data guarantees the preservation of local pavement granular properties. Each profile is modeled as the combination of a large-scale, piecewise smooth function with high-frequency details resulting from the pavement texture. The use of a multiresolution decomposition on an orthogonal wavelet basis allows the separation of these non-correlated physical structures, where the choice of the decomposition level is constrained by the scale ratio of the signal's components.

Since its introduction [6], the multiresolution decomposition has proved to be a particularly efficient tool for analyzing the information content of a signal. Wavelets are families of functions $\Psi_{s,t}(x)$ generated by dilatation s and translation t from the mother wavelet $\Psi(x)$:

$$\Psi_{s,t}(x) = \frac{1}{\sqrt{|s|}}\Psi(\frac{x-t}{s}) \qquad s \neq 0\,, \tag{1}$$

Setting $s = 2^m$ and $t = n$, we get the useful dyadic formulation :

$$\Psi_{m,n}(x) = 2^{-m/2}\Psi(2^{-m}(x-n))\,, \tag{2}$$

where m is the scale parameter and n is the translation index. The 1-D discrete transform $W(m,n)$ is defined as the inner product

$$W(m,n) = \int_{-\infty}^{+\infty} f(x)\,\overline{\Psi_{2^{-m}}(x-n)}\,dx\,. \tag{3}$$

Finite length 1-D signal requires finite decomposition using, at the lower bound of the scale index $m = M-1$, the smoothed version of the signal $S(M,n)$ defined as:

$$S(M,n) = 2^{-M}\int_{-\infty}^{+\infty} f(x)\,\overline{\Phi_{2^{-M}}(x-n)}\,dx\,, \tag{4}$$

where Φ defines the scaling function. Finally, a complete length N representation of a function $f(x)$ is given by:

$$f(x) = \sum_{m=1}^{M} \sum_{n=1}^{2^m} \Psi'_{m,n}(x) W(m,n) + \sum_{n=1}^{M} \Phi(M,n) S(M,N),$$

where $\Psi'_{m,n}(x)$ is the dual basis of $\Psi_{m,n}(x)$ [5]. Since pavement profiles are only composed of 256 points, we use wavelets defined on a short support. A low-order approximation of the low-frequency signal is enough to properly describe its geometry. The separation between low- and high-frequency components can be performed using a few levels of decompositions, that is, a small value of M, since the scale ratio between the signal and its detail space is large. The high-frequency component is then determined by ignoring the coarse scale approximation $S(M,n)$.

2.2 The Haar wavelet.

The Haar function ψ and its scale function ϕ [8], are defined by (see Figure 4)

$$\psi = \begin{cases} 1, & 0 \le x \le \frac{1}{2}, \\ -1, & \frac{1}{2} \le x \le 1, \\ 0, & \text{otherwise}, \end{cases} \quad \phi = \begin{cases} 1, & 0 \le x \le 1, \\ 0, & \text{otherwise}. \end{cases} \tag{5}$$

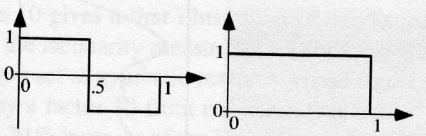

(a) aar function. (b) Scale function.

Figure 4: Haar wavelet.

A family of dilatation and translation, applied to this function, generates an orthogonal wavelet basis. Using eight decomposition levels, the high-frequency component of the data can be separated from a 3 cm piecewise-constant approximation of the profile defined by 32 coefficients at the coarse scale representation. An example of reconstruction of this high-frequency component is illustrated in Figure 5. This example illustrates the elimination of the low-frequency component. We notice a transition of the pavement roughness from a smooth surface to granular surface going from left to right. The presence of two regions of distinctly different roughness natures can be visually detected on the left third and the remainder of the surface respectively.

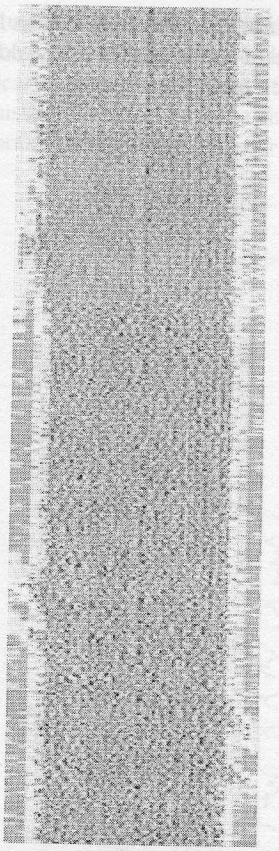

Figure 5: High-frequency component reconstruction for image of Figure 3 (Haar wavelet basis).

2.3 Daubechies wavelets

The orthogonal second-order Daubechies wavelets [9] illustrated in Figure 6 are defined on a short support and allows a better approximation of the profile's coarse scale. Moreover, their orthogonality to polynomial bases ensures a good separation of the singularities of higher order from the low-frequency component of the profiles.

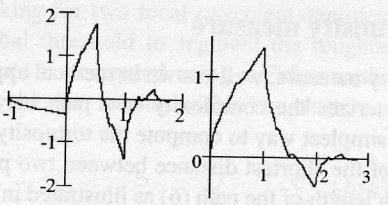

Figure 6: Daubechies wavelet and scale function.

As before, we use an 8-level decomposition. Figure 7 shows the high-frequency component obtained. Although the results seem close to those obtained with a Haar trans-

form, the Daubechies decomposition suffers less in general from the presence of artefacts, since it yields a better approximation of each profile's geometry.

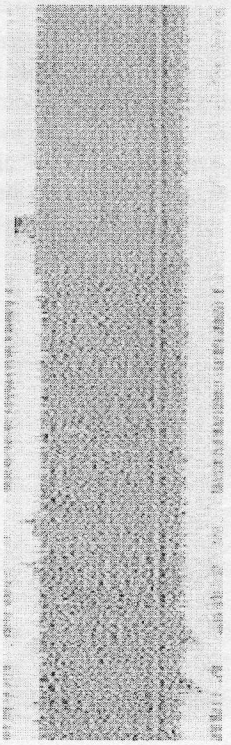

Figure 7: High-frequency component reconstruction for the image of Figure 3 (Daubechies wavelet basis).

3 Roughness estimation

We introduce two methods to compute a roughness index of the local pavement surface. The first one uses each range data profile independently; the second one uses their spatial concatenation.

3.1 Tortuosity measure

The tortuosity measure, well known in medical applications [10], characterizes the complexity of a path between two points. The simplest way to compute the tortuosity measure is the ratio of the shortest distance between two points and the euclidian length of the path (6) as illustrated in Figure 8:

$$\tau \triangleq \frac{\|\vec{AB}\|}{d(AB)_{path}} . \quad (6)$$

Applying the tortuosity measure to the profiles collected along the road segment, we expect a high tortuosity value

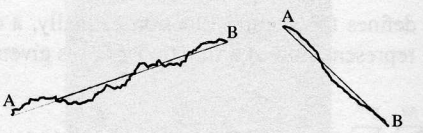

Figure 8: Tortuous paths.

for the complexe signal generated by a granular pavement condition, against a low value for a smooth section. Figure 9 illustrates the tortuosity values obtained with to the image of Figure 7. We observe a large variation of the measure through a transition region located approximatively one third from the left of the image of the pavement texture.This method, however, does not provide a well localized measure of roughness due to its inherent ambiguity. Indeed, a tortuous path of small amplitude and a smooth path of a high amplitude yield similar tortuosity measures. This problem frequently appears when the path length is not large enough to properly describe the signal behaviour.

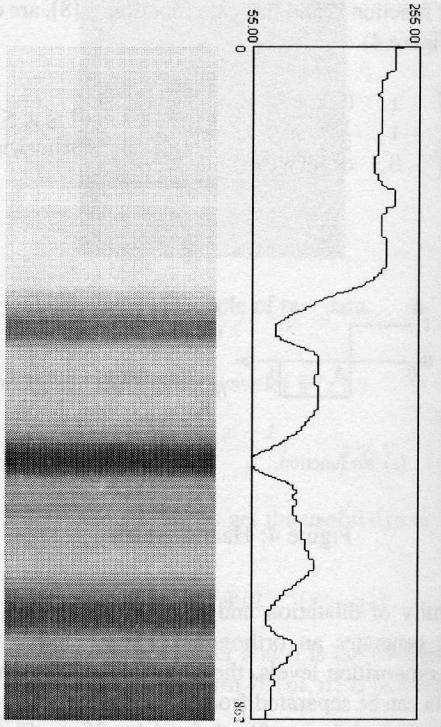

Figure 9: Tortuosity values for image of Figure 7.

3.2 Local lacunarity measure

In this section, we consider the 2-D signal composed from the concatenation of transversal profiles. Relative to the longitudinal (i.e. profile) sampling rate, we assume the piece-

wise continuity of the roughness characteristics of the pavement. The fractal dimension D [11] has been extensively used in segmentation texture analysis [12, 13]. Fractal-based segmentation methods, however, are time-consuming and need sufficiently distinct texture classes to be efficient. Moreover, the fractal dimension does not uniquely define a fractal object [15]. We introduce the lacunarity measure in 7, for a precise discrimination of fractal sets [11, 16, 13]. The choice of this attribute is motivated by the observation that lacunarity is a good estimate of our intuitive notion of surface roughness [13, 14]. Moreover, the implementation of lacunarity is easily derived from a straightforward box-counting fixed-dimension algorithm [17, 18]. The lacunarity is defined as :

$$\Lambda \triangleq E\left(\left(\frac{M}{E(M)}-1\right)^2\right) = \frac{M^2(L)-(M(L))^2}{(M(L))^2}, \quad (7)$$

where

$$M(L)=\sum_{m=1}^{N} mP(m,L),\ M^2(L)=\sum_{m=1}^{N} m^2P(m,L)$$

However, to better adapt estimation to small neighbourhoods, we prefer the following lacunarity formulation [13] :

$$\Lambda(L) \triangleq \frac{M(L)-N(L)}{M(L)+N(L)},\ N(L)=\sum_{m=1}^{N}(1/m)P(m,L). \quad (8)$$

Figure 10 gives a first illustration of the discriminating power of the lacunarity measure. This calculation was performed on a set of synthetic textures whose signal power is reduced by a factor 10 from one class to another. We thus observe a 30 % increase of the lacunarity value with the texture smoothness. Indeed, lacunarity deals with the size of the *holes* of the fractal set. If the fractal object is composed of large gaps, its lacunarity is high. In contrast, the lacunarity is low if the fractal set is almost smooth. On an elevation surface composed of smooth and rough sections, one can expect low lacunarity values in smooth sections against high lacunarity values in granular sections.

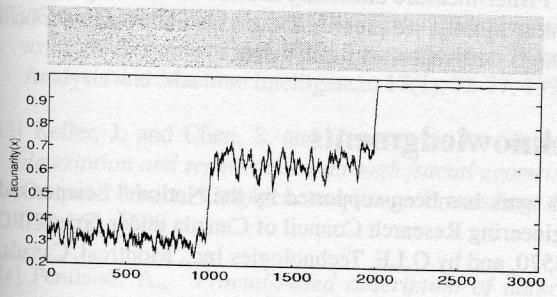

Figure 10: Example of lacunarity values for synthetic data.

Figure 11 illustrates the results of the lacunarity estimation performed on a 12×12 neighbourhoods for the image in Figure 7. We clearly notice the presence of the two sections previously discussed. Despite the large size of the estimation neighbourhood, the separation border is still precisely located.

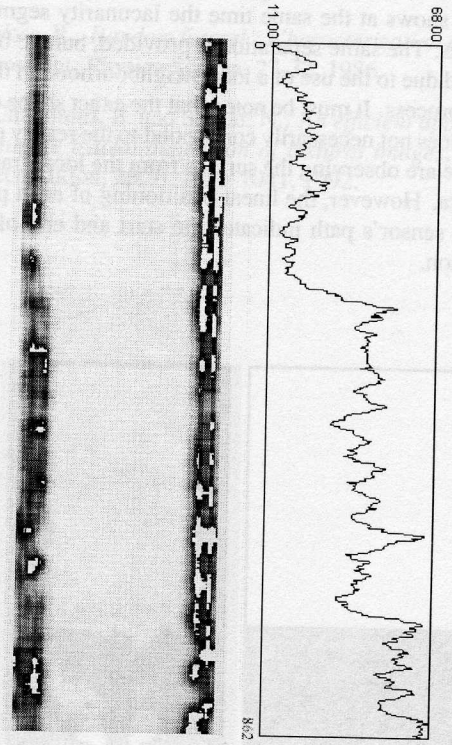

Figure 11: Lacunarity values for image of Figure 7.

4 Classification

The same mono-dimensional clustering technique is used here with the tortuosity and the lacunarity measure. Since we are looking for two local pavement qualities, we use a simple global threshold to segment the roughness values. The threshold is computed using a Fisher method [7], i.e. minimizing the sum inertias within two clusters :

$$S_o \triangleq \arg\min_{s\in\Omega} \sum_{n=1}^{2} \sum_{k\in C_n} h(k)\left(k-\frac{\sum_{k\in C_n} kh(k)}{\sum_{k\in C_n} h(k)}\right)^2, \quad (9)$$

where s is a threshold, S_o is the optimal threshold, $h(k)$ is the value of a variable histogram at index k, and $C_{n=1,2}$ refers to the classes corresponding to threshold s. The

threshold is therefore computed on the normalized histogram of a learning set of tortuosity values then, on the normalized histogram of a learning set of lacunarity values.

The segmentation result in the case of tortuosity is presented on Figure 12(a). The smooth section, in white, is isolated from the coarse roughness surface, in black. Figure 12(b) shows at the same time the lacunarity segmentation results. The same separation is provided, but the border is deviated due to the use of a local neighbourhood in the estimation process. It must be noted that the exact shape of the sections does not necessarily correspond to the reality on the road as we are observing the surface from the local frame of the camera. However, the linear positioning of each profile along the sensor's path indicates the start and end of each road section.

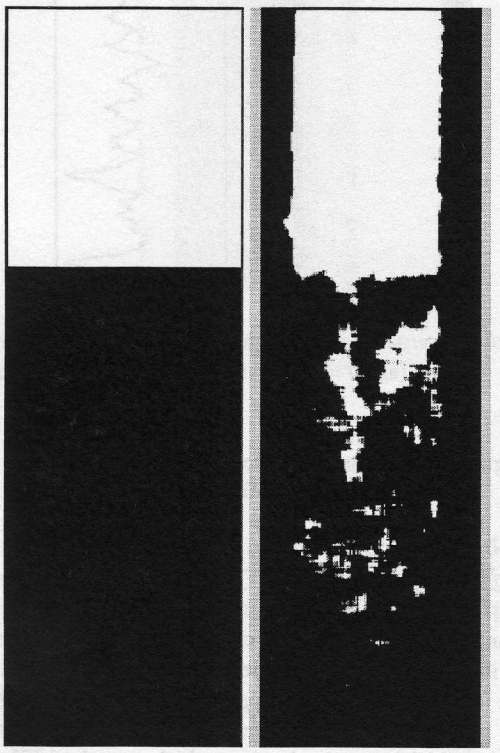

(a) based on tortuosity (b) based on lacunarity

Figure 12: Roughness segmentation.

The main advantage of the lacunarity measure over the tortuosity measure lies in its capability to accurately discriminate between local areas of different roughness characteristics as shown in Figure 13.

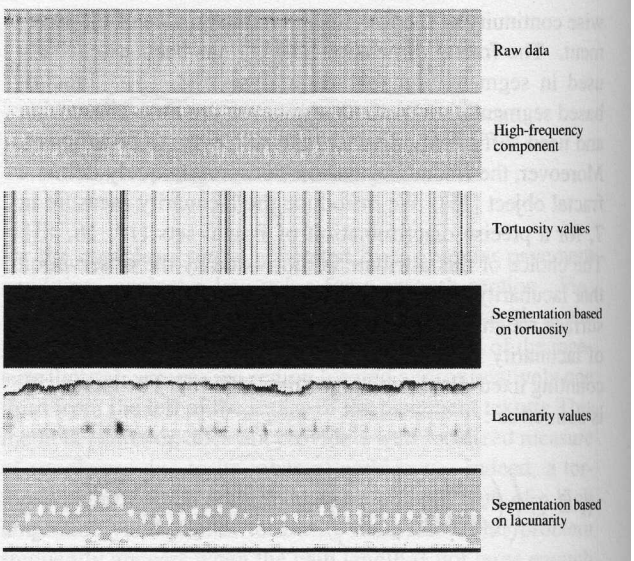

Figure 13: Well localized behavior of lacunarity measure.

5 Conclusions

In this paper we have proposed two segmentation methods to identify pavement sections of distinct roughness characteristics from sequences of range data. Both methods rely on prior decomposition of the range data using the second order Daubechies wavelet transform to extract the high-frequency component related to the pavement texture. Our two approaches differ in the next step, which is the computation of a roughness index for the high frequency component. In the first approach that we presented, the complexity of each profile is characterized using a tortuosity measure. We showed that this method provides an easy way of obtaining a robust segmentation but does not yield a well-localized estimation of the roughness. Next, we proposed a second approach that uses local mass distribution, estimated with the fractal lacunarity measure, as a roughness index leading to a better-localized segmentation. In the last step of our process, we showed how the segmentation of the data into classes of rough and smooth surfaces can by performed by application of a Fisher-measure clustering method to our roughness estimates. Finally, we presented experimental results for both methods with real road surface data.

Acknowledgments

This work has been supported by the National Science and Engineering Research Council of Canada under Grant NRC 193570, and by G.I.E. Technologies Inc., Montreal, Canada.

References

[1] Augereau, B., Khoudeir, M., Brochard, J. and Legeay, V., *Analyse de textures à forte granularité, Application à la reconnaissance de revêtements routiers*, VI/QCAV'99, Trois-Rivières, QC, 1999.

[2] Richard, N., Leard, M. and Legeay, V., *Classification of roadway asphalt by use of fractal signature*, VI/QCAV'99, Trois-Rivières, QC, 1999.

[3] Lecavalier, M. and Blais F., *An Image Processing Accelerator for the BIRIS 3D Vision System. Hardware Functional Specification* Institute for Information Technology. National Research Council Canada, 1994.

[4] Todd, S. and Bursanescu, L., *Vehicle-mounted Imaging System. Measures Road Conditions.* Vision Systems Design, October, 1998.

[5] Mallat S., *A Wavelet Tour of Signal Processing*, Academic Press, Paris, 1998.

[6] Mallat S., *A Theory for multiresolution signal decomposition: The wavelet representation*, IEEE Transactions on Pattern Analysis and Machine Intelligence, **11**(7), July 1989.

[7] Fisher W.D., *On grouping for maximum homogeneity*, JASA, **53**, 789-798, 1958.

[8] Haar, A., *Zur Theorie der Orthoganalen Funktionen-Systeme*, Annals of Mathematics **69**, 331-371, 1910.

[9] Daubechies, I., *Ten lectures on wavelets*, Society for Industrial and Applied Mathematics, 1992.

[10] Hart, W.E., Goldbaum M. and Nelson M., *Automated measurement of retinal vascular tortuosity*, American Medical Informatics Association Annual Symposium, San Diego, CA, 1997.

[11] Mandelbrot, B., *The Fractal Geometry of Nature*, Freeman, New-York, 1983.

[12] Chaudhuri, B. and Sarkar, N., *Texture segmentation using fractal dimension*, IEEE Transactions on Pattern Analysis and Machine Intelligence, **17**(1), 72-77, 1995.

[13] Keller, J. and Chen, S. and Crownover, R., *Texture description and segmentation through fractal geometry*, Conputer Vision, Graphics, and Image Processing, **45**, 150-166, 1989.

[14] Pentland, A., *Fractal-based description of natural scenes*, IEEE Transactions on Image Processing, **6**(6), 661-574, 1984.

[15] Barnsley, M., Devaney, R., Mandelbrot, B., Peitgen, H.O., Saupe, D. and Voss, R., *The Science of Fractal Images*, Springer-Verlag, New-York, 1988.

[16] Mandelbrot, B., *A Fractal's Lacunarity, and How it Can be Tuned and Measured, Fractals in Biology and Medicine*, Birkhäuser-Verlag, Boston, 1995.

[17] Voss, R., *Random fractal : Characterization and measurement*, Physica Scripta, 27-32, 1986.

[18] Chaudhuri, B. and Sarkar, N., *An efficient approach to estimate fractal dimension of textural images*, Pattern Recognition, **25**(9), 1035-1041, 1992.